**ADVANCED
ENERGY
MATERIALS**

Supporting Information

Engineering Temperature-Dependent Carrier Concentration in Bulk Composite Materials via Temperature-Dependent Fermi Level Offset

Si Hui, Wenpei Gao, Xu Lu, Anurag Panda, Trevor P. Bailey, Alexander A. Page, Stephen R. Forrest, Donald T. Morelli, Xiaoqing Pan, Kevin P. Pipe,* and Ctirad Uher*

Supporting Information

Engineering temperature-dependent carrier concentration in bulk composite materials via temperature-dependent Fermi level offset

Si Hui, Wenpei Gao, Xu Lu, Anurag Panda, Trevor P. Bailey, Alexander A. Page, Stephen R. Forrest, Donald T. Morelli, Xiaoqing Pan, Kevin P. Pipe*, and Ctirad Uher*

1. Transport Properties Calculation

For a single parabolic band, the Hall coefficient, Seebeck coefficient, and electrical conductivity can be expressed as below by solving the Boltzmann transport equation with the relaxation time assumption:

$$R_H = \frac{1}{e}\left(\frac{\hbar^2}{2m^*k_BT}\right)^{\frac{3}{2}}3\pi^2\frac{1}{2}\frac{F_{-\frac{1}{2}}(\eta^*)}{\left(F_0(\eta^*)\right)^2} \qquad S1$$

$$\sigma = e^2 w\frac{2}{3\pi^2\hbar^2}\left(\frac{\hbar^2}{2m^*}\right)^{-\frac{1}{2}}k_BTF_0(\eta^*) \qquad S2$$

$$S = \frac{k_B}{e}\left\{2\frac{F_1(\eta^*)}{F_0(\eta^*)}-\eta^*\right\} \qquad S3$$

where e is the elementary charge, $\hbar$ is the reduced Planck's constant, m^* is the effective mass, k_B is the Boltzmann constant, T is the absolute temperature, w is a proportionality constant, $\eta^* = \frac{E_F}{k_BT}$ is the reduced Fermi level, and $F_j(\eta^*) = \int_0^\infty \frac{\eta^j}{1+\exp(\eta-\eta^*)}d\eta$ is the Fermi integral of the jth order. The relaxation time has an energy dependence of:

$$\tau = wE^r \qquad S4$$

where w is a proportionality constant which we set to 1.2×10^{-23} in this work. With acoustic phonon scattering assumed as the dominant scattering process, the scattering parameter r has the value of $-\frac{1}{2}$.

The carrier concentration of a parabolic band can be expressed as:

$$p = \frac{4\pi(2m^*k_BT)^{\frac{3}{2}}}{h^3}F_{\frac{1}{2}}(\eta^*) \qquad S5$$

where h is Planck's constant. The temperature-dependent Fermi level of CuInTe$_2$ is derived from the temperature-dependent Seebeck coefficient of CuInTe$_2$ using this model.

For the case of GeTe, the determination of the transport coefficients is more complicated. It is believed that GeTe has 4-fold degenerate light valence bands at the L point and deeper 12-fold degenerate heavy valence bands at the Σ point with an energy difference of 0.27eV – 0.38eV at 300K.[1-4] Here, we take the value of 0.36eV obtained by Sun et al.[1] The energy difference between the light L band and the heavy Σ band also decreases as the temperature increases,[4-6] so here we take the temperature dependence of the energy difference to be $-1.2 \times 10^{-3} eV/K$ to meet the requirement that the two bands converge at approximately 600K, which was suggested by the Hall coefficient measurement in this work and previous studies.[4,6] The two band model for GeTe can be expressed as:[1]

$$p_l = 4\pi \left(\frac{2m_l^* kT}{h^2}\right)^{3/2} F_{1/2}(\eta_l) \qquad S6$$

$$p_h = 4\pi \left(\frac{2m_h^* kT}{h^2}\right)^{3/2} F_{1/2}(\eta_h) \qquad S7$$

$$\Delta E = (\eta_l - \eta_h) \cdot kT \qquad S8$$

$$S = \frac{p_h}{p_h + p_l \cdot b} S_h + \frac{p_l \cdot b}{p_h + p_l \cdot b} S_l \qquad S9$$

$$S_{l,h} = \frac{k}{e}\left[\frac{2F_1(\eta_{l,h})}{F_0(\eta_{l,h})} - \eta_{l,h}\right] \qquad S10$$

$$R_H = \frac{p_h + p_l b^2}{e(p_h + p_l b)^2} \qquad S11$$

$$\sigma = e(p_l \mu_l + p_h \mu_l/b) \qquad S12$$

where ΔE is the energy difference between the light L band and heavy Σ band, b is the mobility ratio of the light hole to the heavy hole, and μ is the mobility of each band. The subscripts h and l correspond to heavy and light holes, respectively. The temperature-dependent Fermi level of GeTe is derived from the temperature-dependent Seebeck coefficient and electrical conductivity of GeTe using this model.

2. Poisson model

The CuInTe₂ inclusions are assumed to be spheres surrounded by the GeTe phase. The radius of CuInTe₂ inclusions is related to that of the GeTe phase (modeled as spherical for computational convenience) by the doping ratio of CuInTe₂:

$$x = \left(\frac{R_{CIT}}{R_{GT}}\right)^3 \qquad S13$$

where x is the doping ratio. The common energy reference is set as the valence band maximum of pure GeTe. Note that we are studying the effect of holes, so carriers that are deeper into the valence band have higher energy. The spatial distribution of the electrostatic potential $V(r)$ is caused by the charge redistribution after the two phases come into contact and can be determined using the Poisson equation.

For $r \leq R_{CIT}$ in the CuInTe$_2$ region, the Poisson equation can be written as:

$$\frac{1}{r}\frac{d^2}{dr^2}rV(r) = -\frac{e}{\varepsilon_{CIT}\varepsilon_0}p_{CIT-net}(r) \qquad S14$$

For $R_{CIT} \leq r \leq R_{GT}$ in the GeTe region, the Poisson equation can be written as:

$$\frac{1}{r}\frac{d^2}{dr^2}rV(r) = -\frac{e}{\varepsilon_{GT}\varepsilon_0}p_{GT-net}(r) \qquad S15$$

where ε_{CIT} is the dielectric constant of CuInTe$_2$, ε_{GT} is the dielectric constant of GeTe, ε_0 is the vacuum permittivity, $p_{CIT-net}(r)$ is the net charge concentration in the CuInTe$_2$ region, and $p_{GT-net}(r)$ is the net charge concentration in the GeTe region.

At a given temperature, the defect concentrations in GeTe and CuInTe$_2$ determine their carrier concentrations. If a certain amount of free carriers move away from a region, it will be left with net charge which can be written as:

$$p_{net} = p[\mu(r)] - p_0 \qquad S16$$

where $p[\mu(r)]$ is the new carrier concentration determined by the chemical potential $\mu(r)$ after the charge redistribution and p_0 is the carrier concentration under neutral condition before contact, which is determined by the temperature and defect concentration. If we further assume each material possesses a parabolic band structure for simplicity (noting that more complex band structures can easily be implemented), we have from Eqn. S5:

$$p_{net} = \frac{4\pi(2m^*k_BT)^{\frac{3}{2}}}{h^3}\int_0^\infty \frac{\eta^{\frac{1}{2}}d\eta}{1 + \exp\left\{\eta - \frac{E_{F-AC} - E_{VBM-AC}}{k_BT}\right\}} - p_0 \qquad S17$$

with E_{F-AC} and E_{VBM-AC} representing the Fermi level and valence band maximum after the two phases come into contact. Plugging Eqn. S17 into S14 and S15, we have:

For $r \leq R_{CIT}$,

$$\frac{1}{r}\frac{d^2}{dr^2}rV(r)$$

$$= -\frac{e}{\varepsilon_{CIT}\varepsilon_0}\left\{\frac{4\pi(2m_{CIT}k_BT)^{\frac{3}{2}}}{h^3}\int_0^\infty \frac{\eta^{\frac{1}{2}}d\eta}{1+\exp\left\{\eta - \frac{E_{F-AC}-eV(r)-E_{off}}{k_BT}\right\}}\right.$$

$$\left. - p_{CIT-0}\right\} \qquad S18$$

where E_{off} is the energy offset between the maximum of the valence bands of the two phases, and for $R_{CIT} \leq r \leq R_{GT}$,

$$\frac{1}{r}\frac{d^2}{dr^2}rV(r) = -\frac{e^2}{\varepsilon_{GT}\varepsilon_0}\left\{\frac{4\pi(2m_{GT}k_BT)^{\frac{3}{2}}}{h^3}\int_0^\infty \frac{\eta^{\frac{1}{2}}d\eta}{1+\exp\left\{\eta - \frac{E_{F-ac}-eV(r)}{k_BT}\right\}} - p_{GT-0}\right\} \qquad S19$$

In order to solve for V(r) within the domain that we are interested in, additional boundary conditions are needed. At the center of the CuInTe$_2$ inclusion, we set the electric field to be zero, that is:

$$-\frac{dV(r)}{dr}\bigg|_{r=0} = 0 \qquad S20$$

On the other hand, since the total charge within the domain of $r \leq R_{GT}$ is conserved, based on Gauss's law, the electric field at $r = R_{GT}$ is also zero:

$$-\frac{dV(r)}{dr}\bigg|_{r=R_{GT}} = 0 \qquad S21$$

At the interface between the CuInTe$_2$ and GeTe phases, the discontinuity of the electrostatic potential depends on the interface dipole, which is material dependent. Also, the electrical field discontinuity is decided by the interface free charge density. Here, for simplicity, we set them both to zero. Thus, the third and fourth boundary conditions at the interface are:

$$V(r = R_{CIT}^-) - V(r = R_{CIT}^+) = 0 \qquad S22$$

$$-\varepsilon_{CIT}\frac{dV(r)}{dr}\bigg|_{r=R_{CIT}^-} = -\varepsilon_{GT}\frac{dV(r)}{dr}\bigg|_{r=R_{CIT}^+} \qquad S23$$

We used the fourth-order Runge-Kutta algorithm with the shooting method to numerically solve the Poisson equation with the above boundary conditions. To estimate the bulk matrix carrier concentration change due to charge transfer, we divide the total amount of charge transferred across the interface by the total volume of the sample, effectively averaging the charge transfer effect. The material parameters used in the calculation are: $m_{GT} = 0.5m_e$, $m_{CIT} = 5m_e$, $\varepsilon_{GT} = 37.5$,[7] and $m_{CIT} = 10$.[8]

To rule out the influence of interface states on the matrix carrier concentration, we estimated the total number of charge carriers that are trapped by these interface states and calculated the average matrix carrier concentration drop caused by this trapping. We then compared this value (caused by interface states trapping) to the value calculated using the charge transfer model developed above.

The density of interface states is needed to calculate the total number of the charge carriers that are trapped by interface states. We use 10^{14} cm^{-2}eV^{-1} as an estimate for the density of interface states (σ_i).[9] The energy barrier between the interface states and the valence band of GeTe matrix (ϵ_i) is set to 0.05 eV based on the observed convergence of the carrier concentrations of pure GeTe and GeTe-CuInTe$_2$ composites at approximately 600 K (which corresponds to an excitation energy of approximately 0.05 eV). The shape of the nanoscale CuInTe$_2$ secondary phases is set to be spherical (with radius r), with each of these phases embedded in a sphere of GeTe with larger radius (R). Therefore, for the sample with 5% CuInTe$_2$ incorporated, the relation between r and R is:

$$\frac{r^3}{R^3} = 5\% \qquad S24$$

The total number of charge carriers that are trapped in the interface states is $4\pi r^2 \sigma_i \epsilon_i$. Dividing the total number of charge carriers trapped in interface states by the volume of GeTe matrix, the carrier concentration drop in the matrix is:

$$\frac{4\pi r^2 \sigma_i \epsilon_i}{\frac{4}{3}\pi R^3 - \frac{4}{3}\pi r^3} \qquad S25$$

Setting the radius of the CuInTe$_2$ to be 5 nm, the estimated drop in carrier concentration drop is 1.58×10^{18} cm^{-3}.

For the charge transfer model we developed in the paper, with 5% CuInTe$_2$ incorporated in the GeTe matrix, 5 nm radius CuInTe$_2$ spherical inclusions, and 0.4 eV Fermi level offset as determined from Ultraviolet Photoemission Spectroscopy, the total carrier concentration drop in the GeTe matrix is predicted to be 1.0864×10^{19} cm^{-3}.

Comparing the two values calculated using two different models, we find that the carrier concentration drop caused by the interface states is almost an order of magnitude smaller than that caused by the charge transfer. Furthermore, the value we assumed for the density of interface states is an overestimate. We used 10^{14} cm^{-2}eV^{-1} as the value to estimate the density of the interface states, which is an upper bound for the density of surface states. Because atoms at the surface have more dangling bonds than those at the interface, a previous study found the density of interface states to be even smaller (approximately 10^{13} cm^{-2}eV^{-1}).[10] With this value as an estimate for the density of the interface states, the carrier concentration drop in the GeTe matrix caused by interface state trapping is almost two orders of magnitude smaller than that caused by the charge transfer.

3. Sample Structural Characterization

The densities of all samples as measured by the Archimedes method are given in Table S1. All GeTe-rich samples (with GeTe concentrations greater than or equal to 70 mol%) have densities above 6.07 g/cm^3, while CuInTe$_2$-rich samples (with GeTe concentrations less than or equal to 30 mol%) have densities below 5.88 g/cm^3. The theoretical density can be calculated as below, assuming the phases are separated:

$$\rho = \frac{\rho_{CuInTe_2}\left(1 + \frac{m_{CuInTe_2} \times (1 - x\%)}{m_{Ge_2Te_2} \times x\%}\right)}{\frac{\rho_{CuInTe_2}}{\rho_{GeTe}} + \frac{m_{CuInTe_2} \times (1 - x\%)}{m_{Ge_2Te_2} \times x\%}} \qquad S24$$

where ρ_{CuInTe_2} is the theoretical density of CuInTe$_2$, ρ_{GeTe} is the theoretical density of GeTe, m_{CuInTe_2} is the molecular mass of CuInTe$_2$, $m_{Ge_2Te_2}$ is the molecular mass of Ge$_2$Te$_2$, and x is the concentration of GeTe in the composites. Using literature values for the theoretical densities of GeTe (6.14 g/cm^3)[11] and CuInTe$_2$ (6.07 g/cm^3)[12], the calculated theoretical densities of the composites and corresponding relative densities are also listed in Table S1. All GeTe-rich samples have relative densities above 98.9%.

The powder X-ray diffraction (PXRD) patterns of 5 selected samples (GT-100, GT-90, GT-70, GT-30, and GT-10) are presented in Figure S1. The major phase of all the samples is identified as GeTe, with traces of the secondary phases of CuInTe$_2$ and Ge according to the known peak positions of the minerals (GeTe: PDF card ref. 06-0469; CuInTe$_2$: PDF card ref. 06-0605; Ge: PDF card ref. 03-0478). Several major Cu β diffraction peaks arising due to the strong Cu β radiation of the X-ray source are also identified and labeled in Figure S1. As the concentration of CuInTe$_2$ increases, the intensity of the CuInTe$_2$ peaks increases, while that of the GeTe peaks decreases. The Ge impurity peak disappears for all CuInTe$_2$-added samples, indicating that the amount of Ge falls below the detection limit of PXRD. The coexistence of GeTe and CuInTe$_2$ peaks confirms that GeTe and CuInTe$_2$ can only form composites, due

to the different space group of the two compounds (CuInTe$_2$ has a tetragonal structure with the space group I$\bar{4}$2d, while GeTe crystallizes with a rhombohedral structure in the space group $R4m$).[11,12] The secondary phase of Ge is present because Ge forms as a consequence of native defects in GeTe.

Backscattered electron (BSE) images of the GT-98, GT-95, GT-90, and GT-70 samples taken to confirm phase separation are presented in Figure S2. The contrast of light and dark regions in the BSE images clearly confirms the existence of two phases, with the light-colored regions associated with the CuInTe$_2$ phase (which has a larger average atomic weight of 433.566) and the dark background associated with the GeTe matrix (which has a smaller average atomic weight of 400.460). This is confirmed by energy dispersive X-ray spectroscopy (EDS) element mapping, shown in Figure 3a, where the target element accumulates in the lighter area. A small amount of pure Ge is detected in the Ge mapping image as a very light spot that corresponds to a dark spot in the Te mapping image, though the concentration of Ge is so small that PXRD is not able to detect it. No In- or Cu-rich secondary phases were detected in the region tested. Comparing the BSE images of GT-98 and GT-95 in Figures S2a and S2b, it is clear that the concentration of light CuInTe$_2$ areas increases from the former to the latter. The segregation of CuInTe$_2$ in GT-98 strongly indicates that the solubility of Cu and In in GeTe is below 2%. Macroscale BSE images of GT-90 and GT-70 are presented for comparison (Figures S2c and S2d). The sizes of the CuInTe$_2$ inclusions in the GT-70 sample vary from several micrometers to 50 micrometers, and the various shapes of the segregated phase are identified with different surface area to volume ratios. As the concentration of CuInTe$_2$ decreases from 30 mol% to 10 mol%, the extent of segregated CuInTe$_2$ also decreases, and the inclusion shapes tend to be more spherical.

The temperature-dependent heat capacity clearly indicates that a phase transition has taken place at approximately 660 K for all CuInTe$_2$-incorporated composites (Figure 6a). The phase transition temperature of pure GeTe (approximately 674 K) is approximately 15 K higher than that of the composites. The decreased phase transition temperature of the composites suggests that a small amount of Cu and In go into the GeTe lattice to alter the phase transition temperature, as has been observed in a previous study on In-doped GeTe.[1] However, the phase transition temperature shift in our samples is only approximately 15 K, which is much smaller than the value observed in In-doped GeTe (125 K),[1] indicating that the amount of Cu and In entering the GeTe lattice is much smaller. Three consecutive heat capacity measurements were also done on the GT-87.5 sample to confirm the repeatability of the measurement (inset of Figure 6a).

4. Mobility Calculation

For the calculation of the mobility from various scattering mechanisms, we use the expression for electrical conductivity:[4,6]

$$\sigma = \frac{e^2}{3\pi^2} \frac{(2m^*)^{\frac{1}{2}}}{\hbar^3} \int_0^\infty \tau_{total}(E,T) E^{\frac{3}{2}} \left(-\frac{\partial f_0}{\partial E} \right) dE \qquad S25$$

where E is the carrier energy, $\tau_{total}(E,T)$ is the total relaxation time from all scattering processes, and f_0 is the Fermi distribution function. The relaxation time from acoustic phonon scattering is:[4]

$$\tau_{ac} = \frac{2\pi\hbar^4 \rho v_l^2}{(2m^*)^{\frac{3}{2}} E_{ac}^2 k_B T E^{\frac{1}{2}}} \qquad S26$$

where ρ is the material density, v_l is the sound velocity of longitudinal acoustic phonons, and E_{ac} is the deformation potential of acoustic phonons. The relaxation time from point defect scattering is:[4]

$$\tau_d = \frac{2\pi\hbar^4}{(2m^*)^{3/2} N_d \Delta^2 E^{1/2}} \qquad S27$$

where N_d is the defect concentration and Δ is a constant characterizing the mass and strain constant contrast between the matrix and point defect. The relaxation time from precipitate scattering is:

$$\tau_i = \frac{(2m^*)^{1/2} R E^{3/2}}{x V_0^2} \qquad S28$$

where R is the precipitate radius, x is the molar concentration of the precipitate, and V_0 is the interfacial potential between the matrix and the precipitate.

To obtain Figure 6b we used $m^* = 0.5\,m_e$, $E_{ac} = 11$ eV, $V_0 = 0.3$ eV, $\Delta = 10^{-47}$, $R = 20$ nm, $\rho v_l^2 = 130$ GPa, and a Fermi level of 0.3 eV with respect to the valence band edge.

Supporting Information References:

[1]   H. Sun, X. Lu, H. Chi, D. T. Morelli, C. Uher, *Phys. Chem. Chem. Phys.* **2014**, *16*, 15570.

[2]   J. E. Lewis, *Phys. Status Solidi. B* **1973**, *59*, 367.

[3]   M. A. Korzhuev, *Physica Status Solidi B-Basic Research* **1982**, *112*, K39.

[4]   D. Wu, L. D. Zhao, S. Q. Hao, Q. K. Jiang, F. S. Zheng, J. W. Doak, H. J. Wu, H. Chi, Y. Gelbstein, C. Uher, C. Wolverton, M. Kanatzidis, J. Q. He, *J. Am. Chem. Soc.* **2014**, *136*, 11412.

[5]   Y. Z. Pei, X. Y. Shi, A. LaLonde, H. Wang, L. D. Chen, G. J. Snyder, *Nature* **2011**, *473*, 66.

[6]   Y. I. Ravich, B. A. Efimova, I. A. Smirnov, *Semiconducting Lead Chalcogenides* Plenum, New York, **1970**.

[7]   R. Tsu, W. E. Howard, L. Esaki, *Phys. Rev.* **1968**, *172*, 779.

[8]   V. Riede, H. Neumann, H. Sobotta, R. D. Tomlinson, E. Elliott, L. Howarth, *Solid State Commun.* **1980**, *33*, 557.

[9]   J. W. Orton, *The Story of Semiconductors* Oxford University Press, New York, **2006**.

[10] H. Sakaki, K. Hoh, T. Sugano, *IEEE T Electron Dev.* **1970**, *Ed17*, 892.

[11] J. Goldak, C. S. Barrett, D. Innes, W. Youdelis, *J. Chem. Phys.* **1966**, *44*, 3323.

[12] R. H. Liu, L. L. Xi, H. L. Liu, X. Shi, W. Q. Zhang, L. D. Chen, *Chem. Commun.* **2012**, *48*, 3818.

Supplementary Tables and Figures

Sample Name	GT-100	GT-98	GT-95	GT-92.5	GT-90	GT-87.5	GT-85	GT-80	GT-70
Density [g/cm^3]	6.099	6.121	6.071	6.130	6.087	6.143	6.122	6.146	6.082
Theoretical Density [g/cm^3]	6.140	6.139	6.136	6.134	6.132	6.131	6.129	6.125	6.118
Relative Density [%]	99.3	99.7	98.9	99.9	99.3	>100	99.9	>100	99.4

Table S1 Measured densities, theoretical densities, and relative densities of $(Ge_2Te_2)_{x\%}(CuInTe_2)_{1-x\%}$ samples.
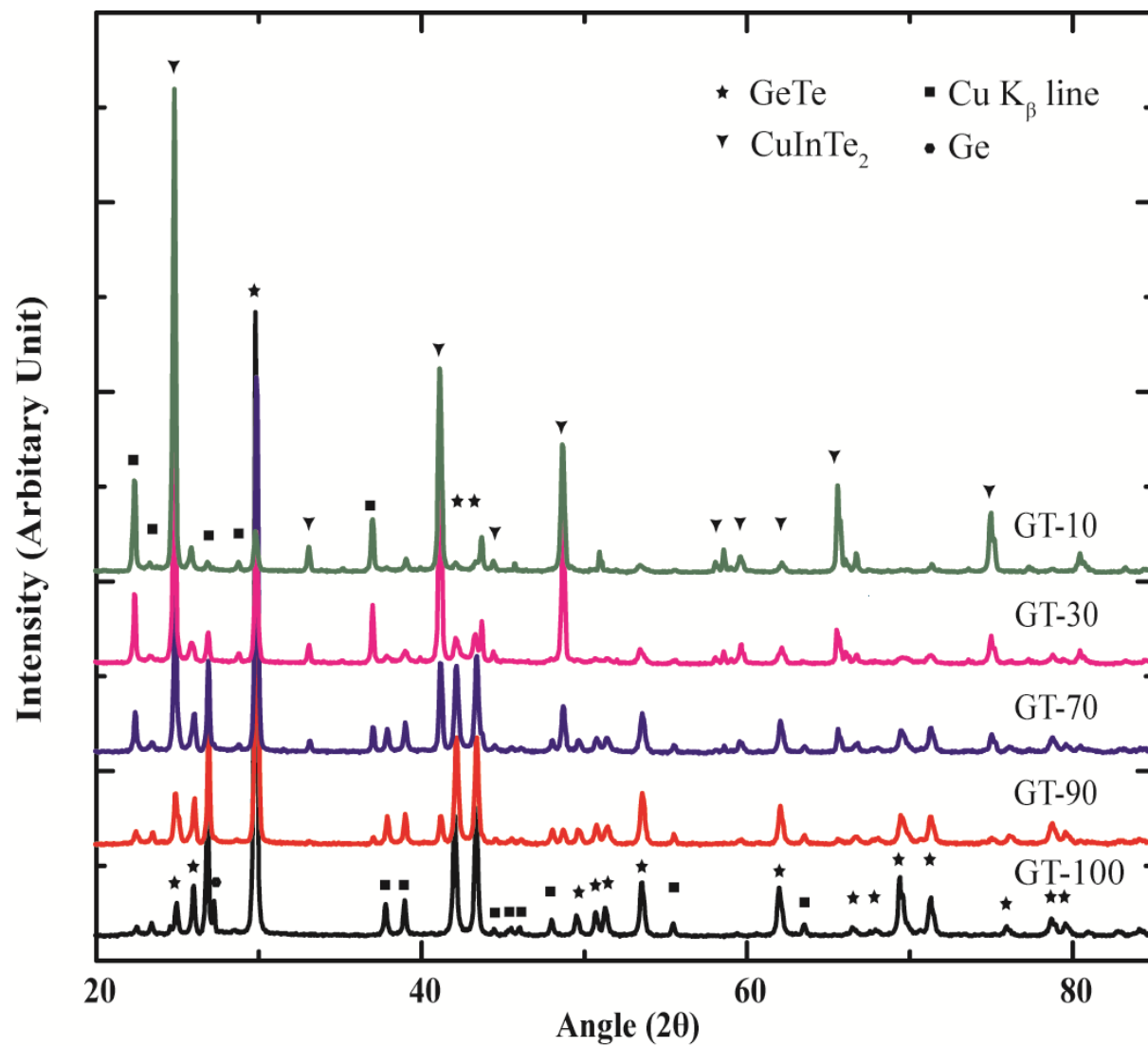
Figure S1 Powder X-ray diffraction patterns of 5 selected samples: GT-100, GT-90, GT-70, GT-30, and GT-10.
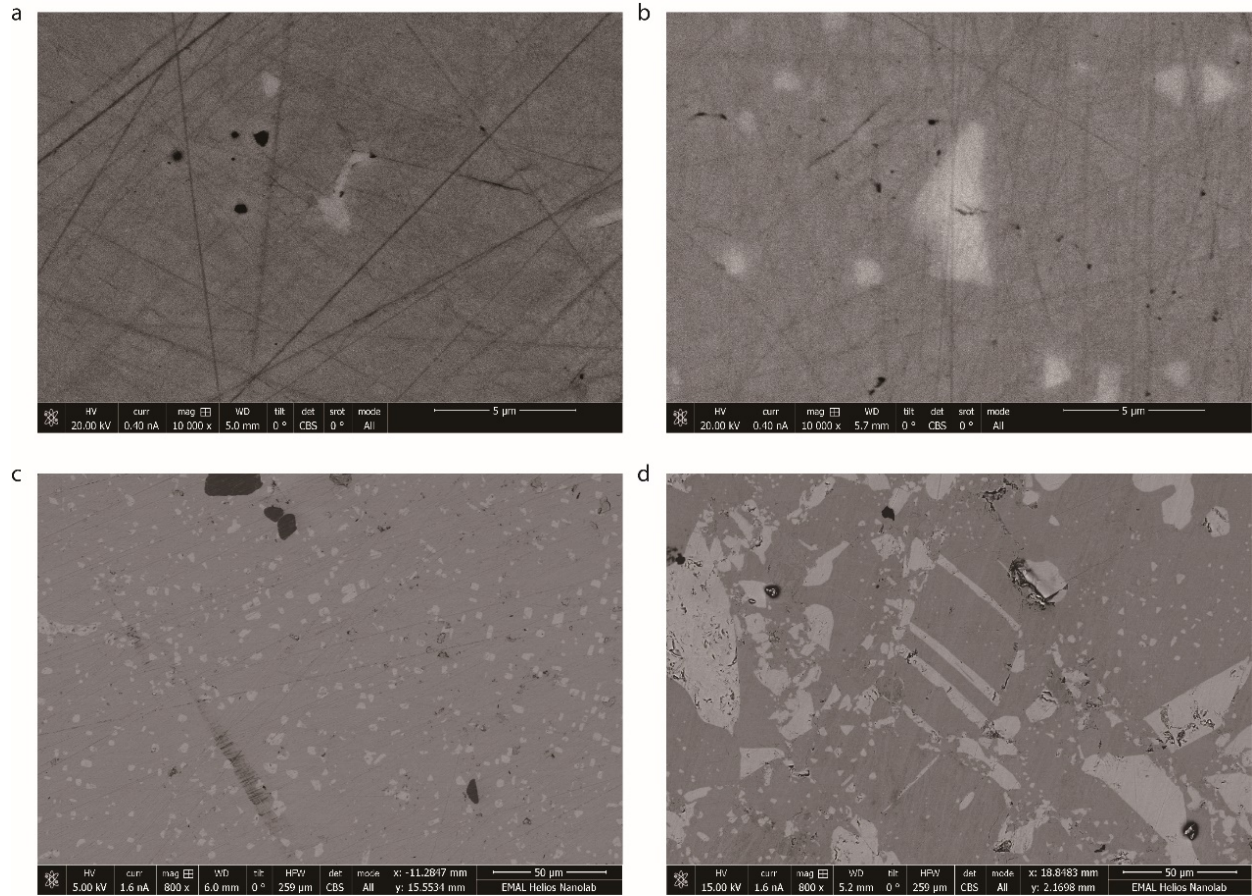
Figure S2 a) Back scattered electron (BSE) image of GT-98 sample with 10000× magnification. **b**) BSE image of GT-95 sample with 10000× magnification. **c**) BSE image of GT-90 sample with 800× magnification. **d**: BSE image of GT-70 sample with 800× magnification.